Paranodal Permeability in "Myelin Mutants"

SEEMA SHROFF,[1] AMANDA MIERZWA,[1] STEVEN S. SCHERER,[4] ELIOR PELES,[5] JUAN C. AREVALO,[3] MOSES V. CHAO,[1,3] AND JACK ROSENBLUTH[1,2*]

[1]Department Physiology & Neuroscience, NYU School of Medicine, New York, New York
[2]Rusk Institute, NYU School of Medicine, New York, New York
[3]Skirball Institute, NYU School of Medicine, New York, New York
[4]Department Neurology, U. Pennsylvania School of Medicine, Philadelphia, Pennsylvania
[5]Department Molecular Cell Biology, Weizmann Institute of Science, Rehovot, Israel

ABSTRACT

Fluorescent dextran tracers of varying sizes have been used to assess paranodal permeability in myelinated sciatic nerve fibers from control and three "myelin mutant" mice, *Caspr*-null, *cst*-null, and *shaking*. We demonstrate that in all of these the paranode is permeable to small tracers (3 kDa and 10 kDa), which penetrate most fibers, and to larger tracers (40 kDa and 70 kDa), which penetrate far fewer fibers and move shorter distances over longer periods of time. Despite gross diminution in transverse bands (TBs) in the *Caspr*-null and *cst*-null mice, the permeability of their paranodal junctions is equivalent to that in controls. Thus, deficiency of TBs in these mutants does not increase the permeability of their paranodal junctions to the dextrans we used, moving from the perinodal space through the paranode to the internodal periaxonal space. In addition, we show that the *shaking* mice, which have thinner myelin and shorter paranodes, show *increased* permeability to the same tracers despite the presence of TBs. We conclude that the extent of penetration of these tracers does not depend on the presence or absence of TBs but does depend on the length of the paranode and, in turn, on the length of "pathway 3," the helical extracellular pathway that passes through the paranode parallel to the lateral edge of the myelin sheath.   © 2011 Wiley-Liss, Inc.

INTRODUCTION

Previous studies have shown that myelin sheaths are attached to axons on both sides of each node of Ranvier by means of a large and highly specialized paranodal axoglial junction (PNJ), which subserves multiple functions (Rosenbluth, 2009). The junction is characterized by a long, narrow junctional cleft traversed by ridge-like "transverse bands" (TBs), thought to be comprised primarily of the axonal contactin/Caspr complex and glial NF155, and responsible for subdividing the axolemma at and around the node of Ranvier into structurally differentiated regions (Rosenbluth, 1976) representing biochemically different "domains" (Poliak and Peles, 2003; Salzer et al., 2008). The permeability of the paranode to macromolecules and ions has been a matter of historical controversy. Prior studies made use of electron microscopic data (Feder, 1971; Hall and Williams, 1971; Hirano et al., 1969; Mackenzie et al., 1984; Reier et al., 1976; Towfighi and Gonatas, 1977), but some of the tracers used, e.g., lanthanum and peroxidase, may not be inert or innocuous and thus could potentially modify the structures they are probing (Feder, 1971), and their localization may also be inaccurate (see Discussion section). In some cases the studies were carried out on fixed tissues and thus might not necessarily reflect the behavior of living nerves.

In order to avoid these issues, a recent study was carried out using fluorescent dextrans. These tracers, which appear to be inert and non-toxic and have been used in studies of extracellular space in the live central nervous system (CNS) (Hrabetova, 2005; Nicholson and Tau, 1993; Thorne and Nicholson, 2006; Sykova and Nicholson, 2008), were employed to test the permeability of the PNJ and Schmidt–Lanterman clefts in mouse sciatic nerve fibers. The results showed some penetration of paranodes by 3 kDa and 70 kDa molecules in both live and fixed nerves (Mierzwa et al. 2010b). These tracers penetrate the paranodes flanking the nodes of Ranvier symmetrically and extend toward the internodal periaxonal space on either side in a time dependent manner, apparently following the helical channel between paranodal loops (pathway 3) rather than passing through the paranodal junctional cleft either axially (pathway 1) or obliquely along the TBs (pathway 2). (See Fig. 1.) In that study, the paranodes examined were all from normal mice, and all components of the PNJ were intact. In view of the possibility that PNJ abnormalities might change paranodal permeability, we have now extended those studies to include mice with genetically determined paranodal defects.
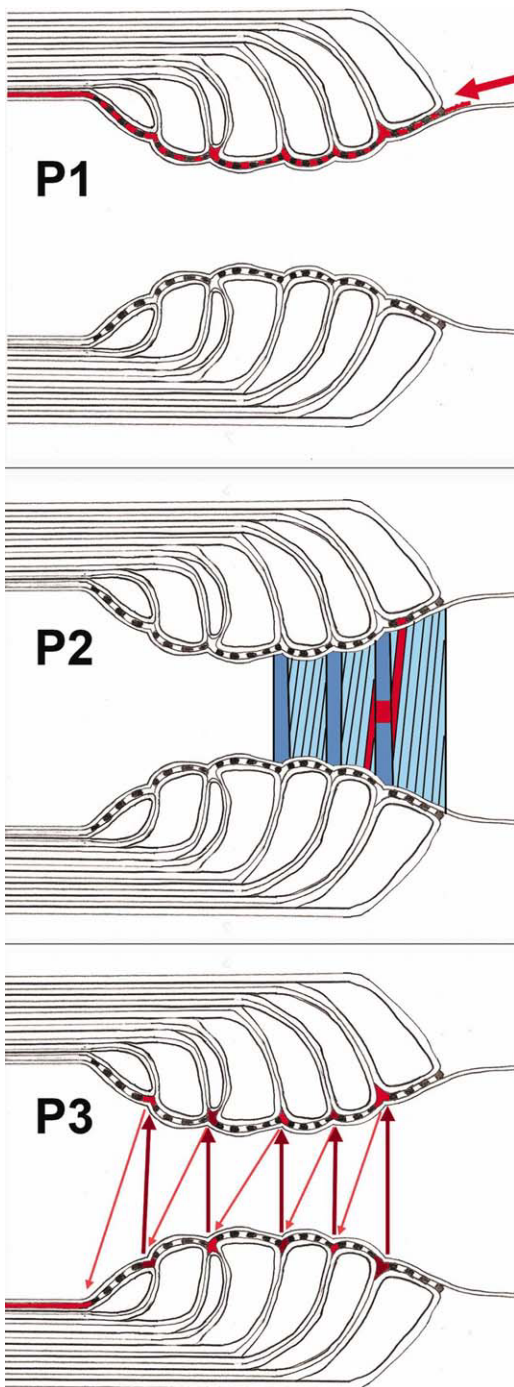
Fig. 1. Postulated pathways (in red) interconnecting the perinodal space with the juxtaparanodal periaxonal space. **Top.** Pathway 1 (P1) beginning at the arrow and passing axially through the paranodal junctional cleft directly across the transverse bands. **Middle.** Pathway 2 (P2) passing obliquely through the paranodal junctional cleft along the transverse bands. **Bottom.** Pathway 3 (P3) passing helically around the axon (arrows) parallel to the lateral edge of the myelin sheath between the paranodal loops and appearing in cross section as a series of triangular profiles. [Color figure can be viewed in the online issue, which is available at wileyonlinelibrary.com.]

A number of these mutants manifest neurological abnormalities including slowed conduction, tremors, tonic seizures, and paresis as well as decreased longevity. Defi-

cient or absent TBs have been shown to be significantly correlated with neurological defects, apparently mediated by defective attachment of the myelin sheath to the axon (Mierzwa et al., 2010a), as a result of which the dimensions of the node and the domain organization of the axon undergo gradual changes leading to progressive conduction defects (Boyle et al., 2001; Coetzee et al., 1996). Two such mutants, *Caspr*-null (Bhat et al., 2001) and *cst*-null (Honke et al., 2002; Ishibashi et al., 2002; Marcus et al., 2006), display significant impairment of their motor functions and shortened lifespan. In contrast, a third mutant, *shaking*, provisionally identified as a *quaking* allele based on cross-breeding studies (Mierzwa et al., 2010a), is much less impaired neurologically and has a normal lifespan. These mutants differ primarily with respect to their complement of TBs, which are absent from the *Caspr*-null mice, present to a very limited degree in the *cst*-null mice but present to a large extent in the *shaking* mice.

Here, we use dextrans to analyze paranodal permeability in these three mutant mice in order to assess the extent to which the permeability of the respective paranodes is altered in relation to their complement of TBs.

MATERIALS AND METHODS
Mice

Control mice used in the dextran experiments were 3–6-month-old C57/Bl6J adults that were housed in the Berg Facility of NYUMC. Age-matched mice from three mutant lines, *Caspr*-null (Gollan et al., 2003), *cst*-null (Honke et al., 2002; Ishibashi et al., 2002), and *shaking* (Mierzwa et al., 2010a) were also used. They were anesthetized with Nembutal and handled in accordance with the IACUC guidelines for NYUMC.

Exposure to Dextrans

Fixed nerves: Mice were anesthetized and sciatic nerves exposed in the thigh; 0.5-cm lengths were excised and immediately immersed in 3% glutaraldehyde/2% paraformaldehyde in 0.1M sodium cacodylate buffer (pH ~7.4) for ~72 h. The nerves were rinsed, stored in tris-buffered saline (TBS, 1×), and used within 2 weeks of excision. The sheath covering a segment of the nerve was slit longitudinally with the point of a 30-gauge syringe needle, and the nerve segment was then submerged in the dextran (diluted to a final concentration of 2–5 mg/mL) in a dark chamber for 1 or 2 h. After six 1-min rinses in TBS, the nerve was laid on a subbed slide in a small drop of TBS, and the fibers were teased apart under a dissecting microscope. The teased preparation was mounted in Vectashield, coverslipped, and visualized with a Nikon fluorescence microscope equipped with Hoffman interference contrast optics. The entire procedure from rinsing through mounting required ~15 min. Because of autofluorescence from the glutaraldehyde fixative, which overlaps rhodamineB fluorescence, only fluorescein-labeled dextrans were used

in this study. The images were analyzed with NIH software, Image J, as described below.

Live nerves: In vivo studies were performed as described in Mierzwa et al. (2010b). Briefly, mice were anaesthetized with Nembutal, and their sciatic nerves exposed. The dextran tracers were injected into the sciatic nerves with a Hamilton syringe and the skin flap sutured back. The mice were monitored for up to 4 h after which they were perfused with 4% paraformaldehyde. The sciatic nerves were then dissected, rinsed, and teased on a subbed slide to be visualized as described above.

Fibers showing tracer penetration were chosen at random in each preparation for photography, and the images were then used for measurement of fiber dimensions and distance penetrated. Fibers showing mechanical damage were excluded.

Dextrans

Fluorescein-labeled or rhodamine-B-labeled dextran powders (Invitrogen) were reconstituted in TBS to a concentration of 10–25 mg/mL, aliquotted, and stored at $-80°$C. For the experiment, these were further diluted (1:5) with TBS. Tracers of four different molecular weights were used: 3 kDa, 10 kDa, 40 kDa, and 70 kDa. Their diameters have been estimated to be $\sim$26Å, 46Å, 90–146Å, and 118–162Å, respectively (Nicholson and Tao, 1993).

Immunohistochemistry

Anesthetized mice were fixed by cardiac perfusion with 1% or 2% cacodylate-buffered paraformaldehyde (pH $\sim$7.3–7.4). Immediately following perfusion, the paraformaldehyde was also injected into the thighs of the animals. After 30 min, the sciatic nerves were dissected out and rinsed in Ringer's solution overnight, then cut into $\sim$1 cm lengths, teased and dried on gelatin-subbed slides, and stored at $-20°$C until used.

Thawed slides were blocked with 10% donkey or goat serum for a minimum of 3 h. Primary antibody was left on overnight. Primary antibodies include αpan Nav (Sigma), αCaspr, and αKv1.2 (Alamone Labs) and K14/16 (Neuromab; www.neuromab.org). After rinsing off primary antibody (3 $\times$ 10 min, 0.1M phosphate buffer), secondary antibody was applied for 1 h and rinsed off in buffer (3 $\times$ 10 min). Secondary antibodies were purchased from Jackson ImmunoResearch. The sections were then covered with anti-fade mounting medium and imaged with a confocal microscope. All measurements were performed using ImageJ software (NIH).

We also studied the distribution of *Stichodactyla helianthus* (SHK) neurotoxin (4,558 Da; Bachem; Devaux and Gow, 2008), which binds K+ channels selectively. Fluorescein isothiocyanate-labeled toxin combined with tetramethylrhodamine-labeled 3 kDa dextran (0.25 mg/mL; Sigma-Aldrich) were diluted in a solution containing (in mM) 126NaCl, 3KCl, 2CaCl$_2$, 2MgSO$_4$, 1.25NaH$_2$-PO$_4$, 26NaHCO$_3$, and 10 dextrose, pH 7.4–7.5. The sciatic nerves of anesthetized adult 129Sv/J mice were exposed, and each nerve was injected subepineurially at three sites with 10 μL at a flow rate of 10 μL/min. The animals were kept for 1 or 2 h under anesthesia and then sacrificed. The sciatic nerves were dissected, teased in cold PBS, dried on glass slides, and mounted with Vectashield medium.

Electron Microscopy

For analysis of sciatic nerve structure and g-ratio measurements, mice were fixed by cardiac perfusion with 3% glutaraldehyde/2% paraformaldehyde in 0.1M cacodylate buffer (pH $\sim$7.3–7.4). Fixative was also injected into the thighs. Sciatic nerves were removed, rinsed, and postfixed in buffered 1.5% potassium ferricyanide/2% OsO$_4$, dehydrated in a graded methanol series, left overnight in propylene oxide, and embedded in Araldite. Thick sections ($\sim$1 μm) stained with alkaline toluidine blue were surveyed by light microscopy and photographed with a digital camera (Nikon CoolPix990). Thin transverse or longitudinal sections ($\sim$0.1 μm) were stained with KMnO$_4$ and uranyl acetate or uranyl acetate alone and imaged with an electron microscope (JEOL JEM-1200 EX II at 80 kV or JEOL JEM-100CX or Philips 300, at 60 kV). For g-ratio studies, electron micrographs of sciatic nerve cross-sections were taken at 10,000$\times$ and digitized. Using Image J software (NIH), a freehand line tool was employed to outline each axon, and the area was determined by an area calculator plugin. This was repeated for the total fiber (axon + myelin). Area values were used to calculate the average diameter of the axon (d) and the axon + myelin (D), and g-ratio was calculated as d/D. The results were segregated into four groups according to axon diameter ($<$2, 2–3.99, 4–5.99, and $>$6 μm). For paranodal structure studies, electron micrographs of longitudinal sections were taken at 5,000–25,000$\times$.

Image Analyses

All fibers were measured in the Hoffman image mode to obtain fiber diameter. The transverse diameter was measured in the internode, away from the paranodal bulge. The Hoffman and fluorescence images were superimposed, and the total extent of dextran penetration on both sides of the node was measured in those images. To calculate the distance penetrated on each side of the node, the length of the node for each genotype (as shown in Table IV) was subtracted from the total penetration and the result divided by 2. Axon diameters (d) were calculated from fiber diameters (D) measured in Hoffman images, and g-ratios derived from electron micrographs (see above) as $d = D \times g$.

Measurement of Paranodal Length by Dextran Distribution

Fibers with clearly labeled paranodes that also showed dextran penetration beyond the paranode (i.e.

those having "hairpin" extensions) were chosen for this study. Axon caliber widens abruptly to form "shoulders" where the paranode adjoins the juxtaparanode, and just at that point the fluorescent paranodal "bar" forms the tines of the "hairpin" extending beyond the juxtaparanode into the internode. In order to obtain paranodal length, we measured the "shoulder-to-shoulder" distance between the distal ends of the two paranodal "bars" flanking the node, i.e. just up to the point where the hairpins began, using the NIH software, Image J. From that value, average measured node length was subtracted and the remainder divided by 2 to obtain average paranodal "bar" length on each side.

Statistics

Statistical analyses were done using a two-tailed Student t-test in Microsoft Excel or GraphPad Prism, version 2.0. A P value of <0.05 was considered significant. The correlation coefficient, r, was calculated using Microsoft Excel software.

RESULTS

Our previous study of normal myelinated fibers (Mierzwa et al., 2010b) showed that tracer movement in glutaraldehyde-fixed specimens corresponds well to that in live-injected specimens. We found much more variation in the live nerves probably because the location of the bolus of tracer injected varied with respect to both the radial position and the longitudinal position of each node examined within the nerve. Thus, the distance diffused by the tracer before it reached the individual nodes varied considerably. In the fixed, soaked preparations, in contrast, only the radial position of each node varied, because the entire length of the nerve was covered uniformly with tracer. In the current study, we have mainly used fixed specimens in order to minimize variation from this source.

Structure of the PNS Paranode

We examined paranodes from the mouse CNS in our study of *shaking* nerve fiber structure (Mierzwa et al., 2010a). Here, we present a brief counterpart description of paranodes from the mouse *peripheral* nervous system (PNS), specifically the sciatic nerve.

As shown in Fig. 2A, *shaking* PNS paranodes are close to normal in overall appearance. Terminal loops indent the axon resulting in the characteristic scalloped appearance of the junctional membrane (Fig. 2B), but compared with CNS terminal loops, those in the PNS tend to extend away from the axon at a much steeper angle, approaching 90° in some cases (Fig. 2A), before the inner surfaces of their limiting membranes fuse to form compact lamellae peripherally. Correspondingly, the extracellular interstices between adjacent loops are

also longer than those in the CNS, but are generally occluded by tight junctions close to their base just above the point where the adjacent Schwann cell membranes curve away from each other to form a roughly triangular "corner" (arrowheads, Fig. 2C; cf., "pathway 3" in Fig. 1) bounded by the respective Schwann cell membranes at its sides, the axolemma at its base and the tight junction at its apex. The apical tight junction is not always present, however, and in those cases the space between the adjacent paranodal loops remains open at the apex of the triangle, extending away from the axon into the paranode.

The paranodal junctional cleft is only several nanometers wide and contains TBs, but as in the CNS, these are somewhat less consistently present in the *shaking* paranodes than in controls. The axial length of each paranodal loop indentation is shorter than that in the CNS, and in addition, many more loops end on other loops and do not reach the axolemma (Fig. 2B). As a result, the overall length of the PNS paranode is shorter than what would be expected based on the number of compact lamellae in the sheath. Microtubules are less conspicuous in the PNS loops than in those of the CNS, and in the *shaking* PNS occasional paranodes display degenerative changes consisting of swelling and organelle accumulation in the inner (abnodal) loops (Fig. 2D).

Tracer Penetration Decreases with Increasing Dextran Diameter

All four fluorescent dextrans, 3 kDa, 10 kDa, 40 kDa, and 70 kDa, penetrated in the same manner in fixed nerves (see Fig. 3) as they did in live-injected nerves, reported previously (Mierzwa et al., 2010b). In addition to being localized to some extent along the outside of the fiber (Fig. 3B and H), the dextrans were also present at the nodal slit and perinodal space (Fig. 3B, E, and H). Each dextran then spread longitudinally in both directions beneath the myelin sheath forming a rod-shaped structure, the "paranodal bar" between the axon and the myelin sheath (Fig. 3H and K).

At longer times, the dextrans penetrated beyond the paranode, into the internodal periaxonal space, often appearing as a pair of tines at the outer edges of the axon (Fig. 3E and K). These "hairpins" probably result from the better visualization of the periaxonal dextran at the tangent of the axonal circumference (Mierzwa et al., 2010b).

To determine the extent of dextran diffusion, we measured the length of visible fluorescence for each tracer along the combined adjacent paranodes/internodes (Table I). In fixed control nerves the average penetration of the 3 kDa and 10 kDa dextrans at 1 h was comparable (3 kDa penetration = 11.2 ± 5.6 μm; 10 kDa penetration = 10.8 ± 4.7 μm). The 40 kDa and 70 kDa dextrans penetrated more slowly and hence were measured at 2 h. They too showed comparable penetration (40 kDa penetration = 10.1 ± 5.0 μm; 70 kDa penetration = 9.7 ± 5.3 μm). As shown in Fig. 4, the 10 kDa dextran penetrated many more myelinated fibers than
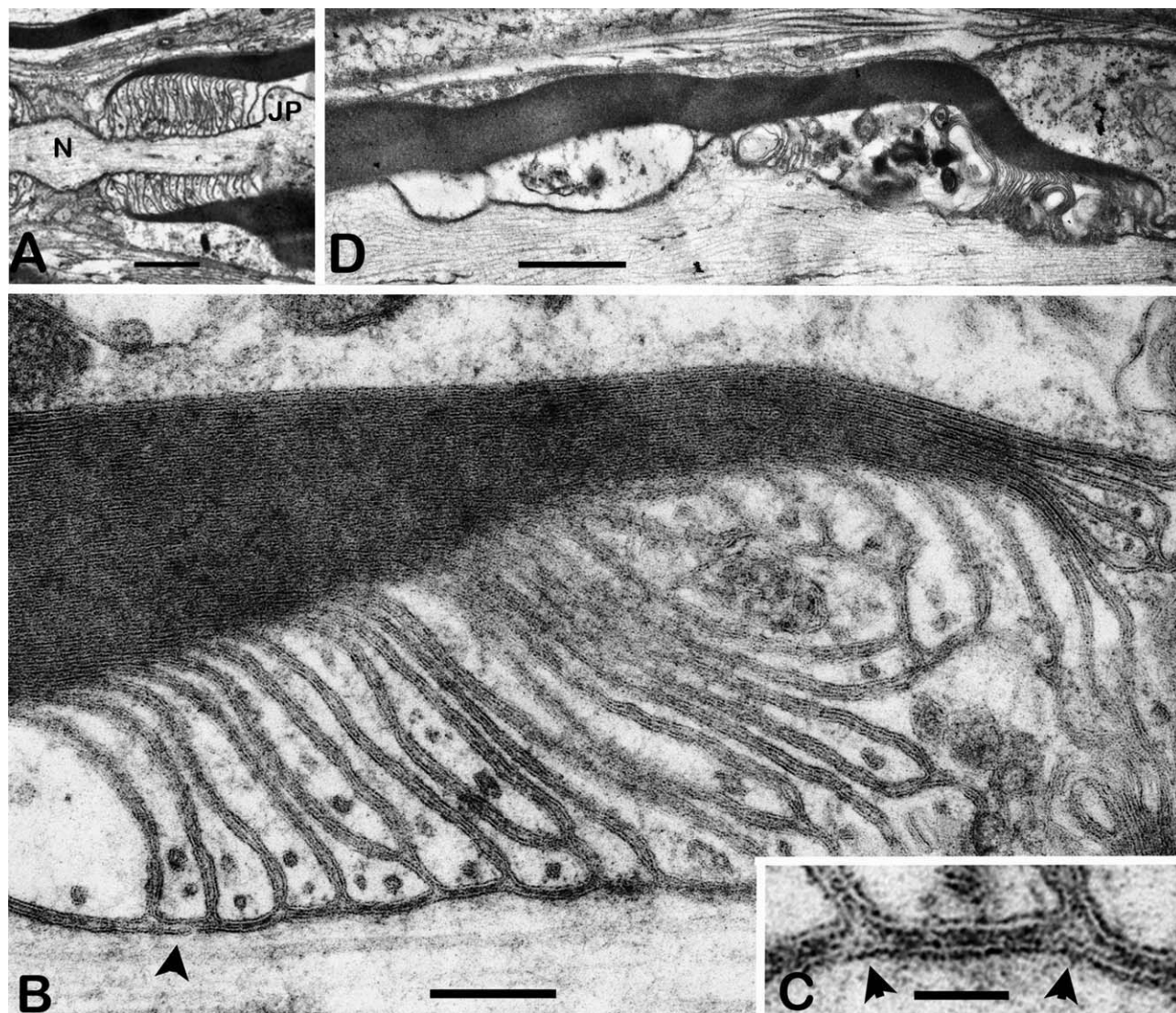
Fig. 2. Paranodal structure in *shaking* sciatic nerve. (**A**) Survey view of a paranode. The axon widens at the node (*N*) and at the shoulder region of the juxtaparanode (JP). Elongated terminal loops of myelin are oriented at ~90° to the axonal axis. Scale bar = 1 μm. (**B**) Portion of a paranode showing terminal loops indenting the axolemma slightly. Transverse bands are associated with most paranodal loops but are absent from some (arrowhead). Many terminal loops do not reach the axolemma. Scale bar = 0.2 μm. (**C**) Detail of B showing two roughly triangular 'corners' (arrowheads) between adjacent terminal loops. (cf., "pathway 3," Fig. 1.) TBs are visible within the junction between the arrowheads and on either side. Scale bar = 0.05μm. (**D**) Degenerative changes (swelling and organelle accumulation) in the inner loops of a myelin sheath adjacent to a paranode (right). Scale bar = 1 μm.

did the 40 kDa dextran, comparable to the disparity between 3 kDa and 70 kDa dextran penetration previously found (Mierzwa et al., 2010b).

When SHK toxin (~4.6 kDa), slightly larger than 3 kDa dextran, was injected into live sciatic nerves in situ, as in optic nerves (Devaux and Gow, 2008) the toxin bound to axons in paired patches separated from each other by a distance corresponding to the length of one node of Ranvier plus the lengths of the two flanking paranodes (Supp. Info. Fig. 2). The location of the labeled patches is thus consistent with that of the juxtaparanodal domains, where Kv1.1 channels, the target of SHK, are enriched. The route by which the toxin reached its target was not visualized, however.

Dextran Penetration is Inversely Proportional to Axon Diameter

In control samples, the average 3 kDa dextran penetration at 1 h in "small" fibers (axon diameter <4 μm) was 14.3 μm on both sides of the node. This figure is higher than the average penetration (11.2 μm) in fibers of all sizes shown in Table II. Average 3 kDa penetration in large fibers (axon diameter >8 μm) was 9.8 μm. This figure is significantly lower than the average penetration in small fibers in the same preparations ($P = 0.02$).

Measured 3 kDa penetration at 1 h with respect to increasing axon diameter reveals a mild but statistically significant negative correlation (coefficient $r = -0.21$,
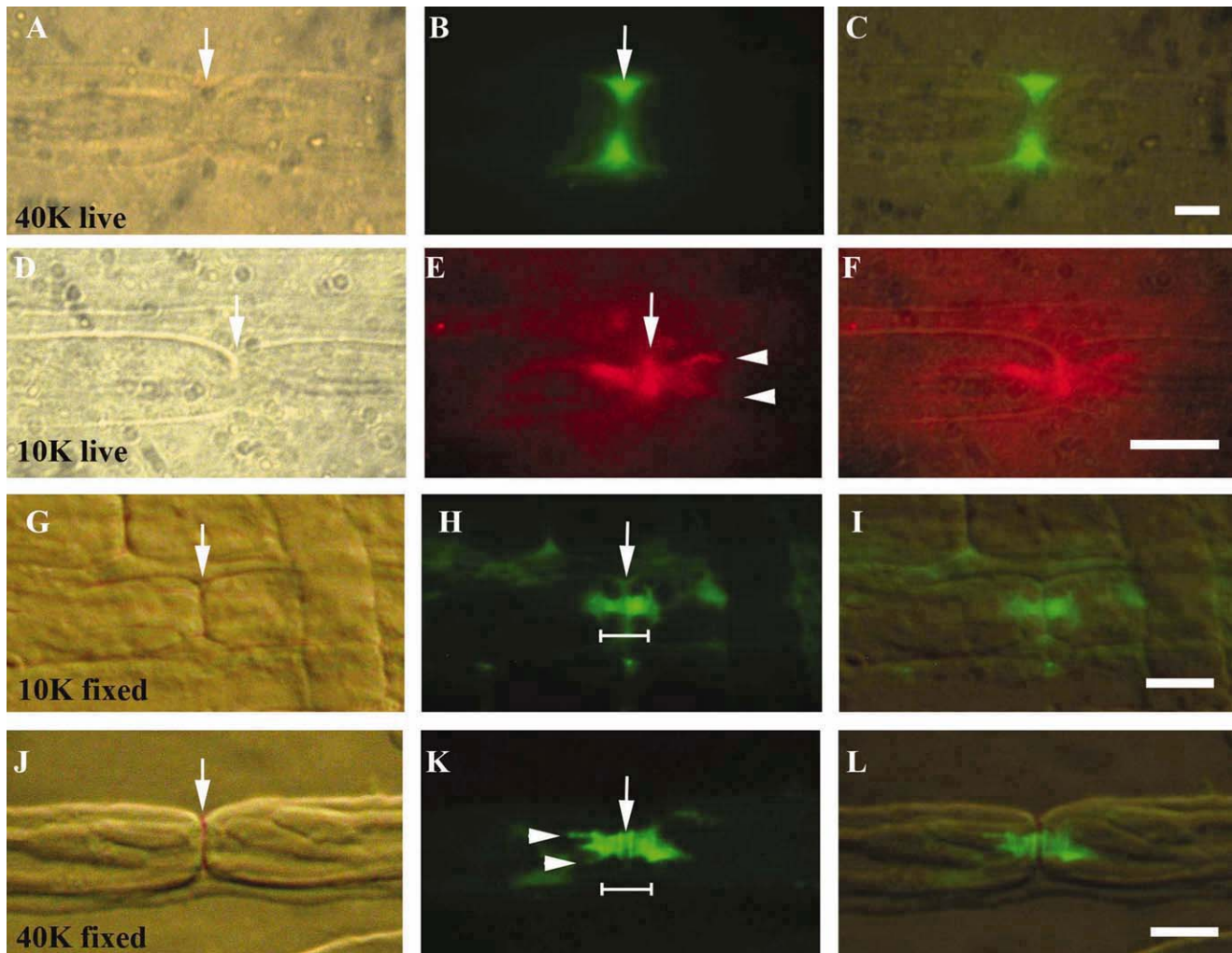
Fig. 3. 10 kDa and 40 kDa dextran tracer penetration in control sciatic nerve fibers. The node of Ranvier is marked by an arrow in (**A**), (**D**), (**G**), and (**J**). Images (**A**–**F**) are from live injected fibers, whereas (**G**–**L**) are from fixed fibers soaked in dextran solution. (A–C) 40 kDa dextran (green). The tracer has pooled in the perinodal space on either side of the nodal slit (arrow, B). Scale bar = 5 μm. (D–F) 10 kDa dextran (red). The tracer has spread from the node of Ranvier (arrow, D and **E**) laterally through the paranode into the internode forming "hairpins" (arrowheads, E). Scale bar = 5 μm. (G–**I**) 10 kDa tracer (green) after 1 h soak showing the nodal slit (arrow, G and H). Paranodal bar in H widens at its abnodal ends at the junction with the internode (shoulder). Scale bar = 10 μm. (**J**–**L**) 40 kDa tracer (green) showing paranodal bar and hairpins (arrowheads in K) after 2 h soak. The tracer is sometimes washed out of the node slit, which then appears dark (arrow, K). Scale bar = 10 μm. [Color figure can be viewed in the online issue, which is available at wileyonlinelibrary.com.]

$P < 0.01$, $n = 238$). Because paranode length also changes with axon caliber, both axon diameter and paranode length could underlie the difference in penetration.

The contribution of paranode length is likely to be small, however, because in normal fibers paranode length varies within a very narrow range. This is partly because with

TABLE I. *Mean Penetration of Different Size Dextrans in shaking* and Control Mice

	# mice	# nodes	Fiber diam.	Axon diam.	Penetration μm ± SD (both sides)	P
3 kDa (1 h)WT	15	238	9.1 ± 1.9	6.4 ± 1.5	11.2 ± 5.6	
shaking	12	179	8.2 ± 1.8[a]	6.5 ± 1.6	22.1 ± 9.7[c]	6.5×10^{-32}
10 kDa (1 h) WT	4	110	8.7 ± 1.8	6.1 ± 1.4	10.8 ± 4.7	
shaking	4	55	8.0 ± 1.4[a]	6.4 ± 1.3	15.4 ± 6.3[c]	5×10^{-6}
40 kDa (2 h) WT	4	55	8.8 ± 1.8	6.1 ± 1.4	10.1 ± 5.0	
shaking	4	30	7.5 ± 1.9[a]	5.8 ± 1.7	14.0 ± 6.0[b]	0.004
70 kDa (2 h) WT	23	207	8.8 ± 2.2	6.2 ± 1.7	9.7 ± 5.3	
shaking	17	123	7.8 ± 1.7[a]	6.2 ± 1.5	14.1 ± 7.6[c]	4×10^{-8}

Axial dextran penetration (both sides) was measured in randomly chosen, teased sciatic nerve fibers from 3 to 7 month *shaking* and control mice at 1 h (3 kDa and 10 kDa) or 2 h (40 kDa and 70 kDa). Axon diameters were individually calculated using g-ratios from Supp. Info. Fig. 1. Penetration by all four dextrans is increased ~1.4–2× in *shaking* axons vs controls.
[a]$P < 0.05$.
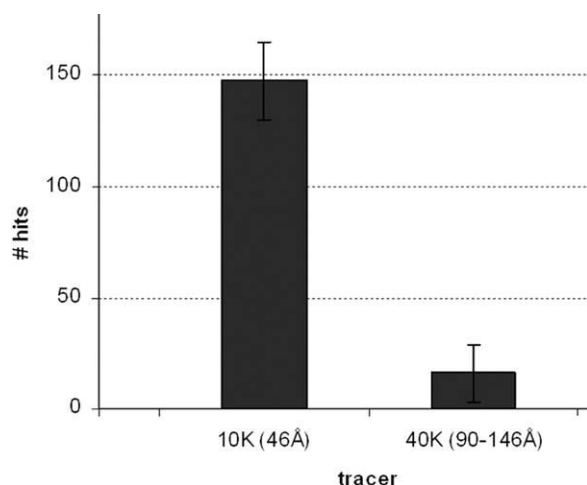[b]$P < 0.01$.
[c]$P < 0.001$.

Fig. 4. Number of control sciatic nerve fibers penetrated by different size dextrans. Bar graph showing number of nodes labeled by dextran tracers (hits) in a teased preparation from a ~0.5-cm piece of fixed sciatic nerve soaked in tracer solution for 2 h. The 10 kDa tracer penetrates ~9× as many nodes as the 70 kDa tracer.

increasing fiber diameter, myelin sheaths are comprised of progressively larger numbers of lamellae, but in the paranode increasingly larger numbers of paranodal loops end in clusters *not* in direct contact with the axolemma (Fig. 2B). Thus, the number of paranodal loops contacting the axolemma to form paranodal junctions does not increase in proportion to the total number of myelin lamellae. Hence, the relation between paranode length and axon diameter is highly non-linear, especially in the case of large-caliber PNS fibers (Berthold and Rydmark, 1983; Bertram and Schroder, 1993; Shepherd et al., 2010).

Dextran Penetration is Independent of TBs

To determine whether TBs affect dextran penetration, we used three mutant mice with varying expression of TBs in their paranodes and compared them to controls. TBs are present in large numbers in the CNS of *shaking* mice (~60% normal; Mierzwa et al., 2010a) and are abundant in the PNS as well (Fig. 2B and C), but *cst*-null mice have only rare TBs (Hoshi et al., 2007; Marcus et al., 2006), and none have been seen in *Caspr*-null mice, either from the line generated by Bhat et al. (2001) or the line generated by Gollan et al. (2003) that we used. As summarized in Tables II and III the penetration of 3 kDa dextran at 1 h or 70 kDa dextran at 2 h was not significantly increased in either *Caspr*- or *cst*-null mice over that in control mice. Thus, transverse bands do not impede the diffusion of these dextrans.

Dextran Penetration is Increased in the *Shaking Mutant*

Surprisingly, the *shaking* mutant, which has the most TBs of the three mutants, showed *increased* penetration of the 3 kDa and 70 kDa dextrans (1.4–2× controls), as shown in Tables II and III. Because the average caliber of myelinated fibers in *shaking* sciatic nerves is significantly smaller than that in controls (Table I), the increased penetration could be related to a smaller average axon diameter (see above). We evaluated this possibility by measuring axonal dimensions and myelin sheath thickness in electron micrographs, thereby obtaining *g*-ratios. These are significantly higher in *shaking* than in controls; i.e. *shaking* myelin is thinner (Supp. Info. Fig. 1), presumably because of myelin instability (Fig. 2D) and remyelination (Mierzwa et al., 2005). Because the fiber caliber is based on both axon diameter and myelin thickness, we calculated axon diameters based on the *g*-ratios in *shaking* and control sciatic nerves and found that the average axon diameter in the *shaking* population is, in fact, equal to that in controls (Table I).

To determine whether the paranodes might be shortened in *shaking* mutants, we immunostained teased fibers for Caspr. In 1-month mice, *shaking* paranodes are 24% shorter than those in controls (1.7 ± 0.1 μm, $n = 22$ vs 2.3 ± 0.2 μm, $n = 48$; $P = 0.001$). A similar trend (16% shorter) was found in older (6–7.5 month) animals (2.16 μm, $n = 13$ vs 2.58 μm, $n = 19$), but, in the smaller sampling in this case, that difference did not reach statistical significance (Mierzwa et al., 2010a). Using "shoulder-to-shoulder" measurements of paranodes outlined by dextran (Fig. 5

TABLE II. *Mean 3 kDa Dextran Penetration in Different Mutants at 1 h*

	WT	*Caspr*-null	*cst*-null	*shaking*
# mice	15	2	2	12
# nodes	238	33	41	179
Mean fiber diam. μm ± SD	9.1 ± 1.9	9.5 ± 2.0	8.8 ± 1.6	8.2 ± 1.8[a]
Mean penetration μm ± SD (both sides)	11.2 ± 5.6	11.4 ± 3.8	9.3 ± 3.5[a]	22.1 ± 9.7[b]
P value		0.79n.s.	0.004	6.5×10^{-32}

Mean penetration (both sides) in fibers of all sizes, measured in teased preparations from WT, *Caspr*-null, *cst*-null and *shaking* mutants. Overall caliber of myelinated fibers measured from the Hoffman images, is approximately the same in WT, *Caspr*-null, and *cst*-null mutants. *Shaking* fibers show a significantly reduced fiber diameter because their myelin sheaths are thinner (see text). The 3 kDa tracer penetration at 1 h in the *Caspr*-null mice is comparable to normal, slightly reduced in the *cst*-null mice and almost double in the *shaking* mice. P values show significance in mutant vs WT measurements.
[a]$P < 0.05$.
[b]$P < 0.001$.

TABLE III. *Mean 70 kDa Dextran Penetration in Different Mutants at 2 h*

	WT	*Caspr*-null	*cst*-null	*shaking*
# mice	23	9	7	17
# nodes	207	160	92	123
Mean fiber diam. μm ± SD	8.8 ± 2.2	8.5 ± 2.0	8.7 ± 1.7	7.8 ± 1.7[a]
Mean penetration μm ± SD (both sides)	9.7 ± 5.3	9.8 ± 5.8	10.3 ± 4.6	14.1 ± 7.6[b]
P value		0.89n.s.	0.33n.s.	4×10^{-8}

Mean penetration (both sides) in fibers of all sizes, measured in teased preparations from WT, *Caspr*-null, *cst*-null, and *shaking* mutants. Penetration at 2 h in the *Caspr*-null and *cst*-null is comparable to that in controls but significantly increased in the *shaking* mutant. P values show significance in mutant vs WT measurements.
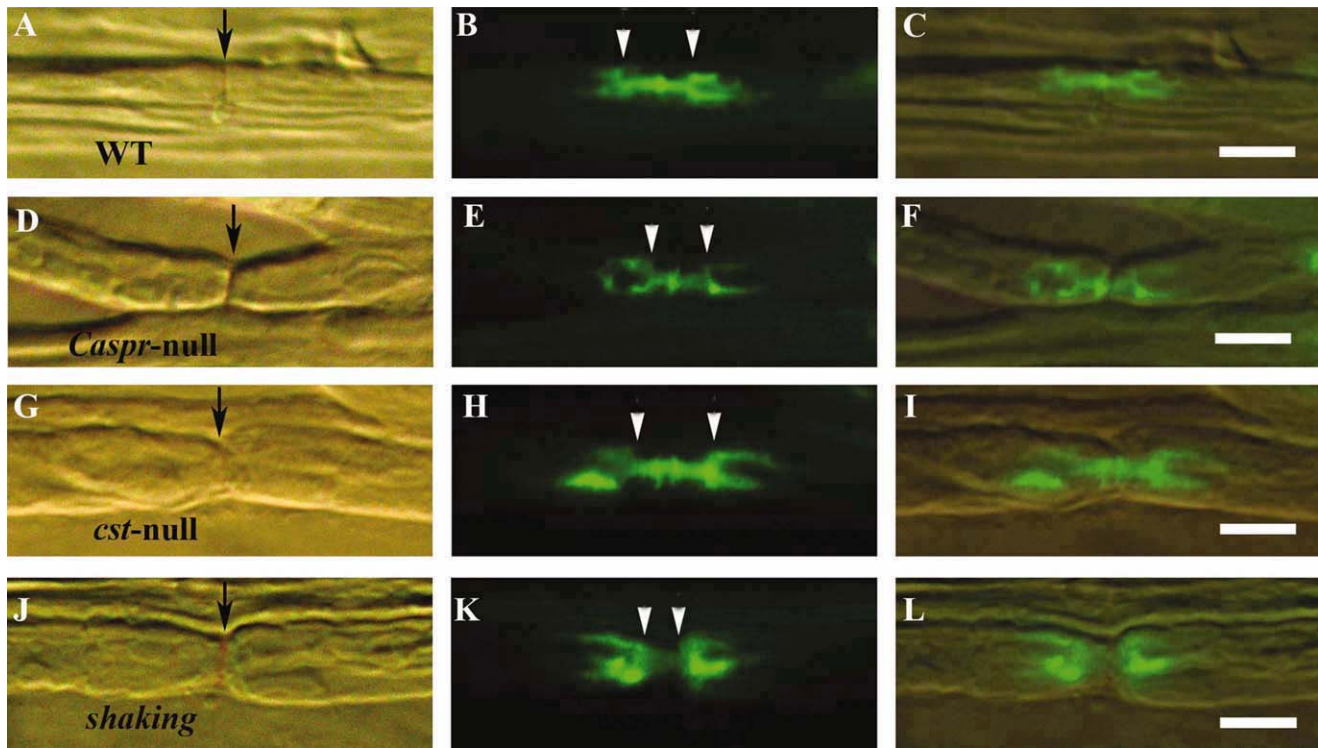[a]$P < 0.05$.
[b]$P < 0.001$.

Fig. 5. Paranodal length in control and mutant sciatic nerve fibers. 3 kDa tracer (green) in fixed fibers after 1 h soak from WT (**A–C**), *Caspr*-null (**D–F**), *CST*-null (**G–I**), and *shaking* (**J–L**) mice. The length of the paranodal bar (both paranodes + the intervening node) was measured from the point of widening (shoulder) of the tracer outline (arrows, B, E, H, and K). The *shaking* fibers have the shortest paranodes. The node of Ranvier is shown by arrows in (A), (D), (G), and (J). Scale bar = 10 μm. [Color figure can be viewed in the online issue, which is available at wileyonlinelibrary.com.]

TABLE IV. Paranode Length in Mutant vs Control Sciatic Nerves

	WT	*Caspr*-null	*cst*-null	*shaking*
# mice	12	3	3	11
# nodes	65	43	48	76
Mean fiber diam.	8.3 ± 1.8	7.4 ± 1.9	8.1 ± 1.9	7.9 ± 1.8
Mean PN bar length μm ± SD (both sides)	7.0 ± 1.4	6.5 ± 2.2	7.7 ± 2.3	5.4 ± 1.7[a]
Node length (μm)	0.8	1.1[a]	1.7[b]	0.9
Mean PN length μm ± SD (one side)	3.1 ± 0.7	2.7 ± 1.1	3.0 ± 1.1	2.3 ± 0.8[c]

Mean length of the "paranodal bar" (both sides) was measured in fibers of comparable size in WT, *Caspr*-null, *cst*-null, and *shaking* mouse sciatic nerves. The average length of each paranode (one side) was then calculated by subtracting node length and dividing the remainder by 2. *Shaking* paranodes are ~27% shorter than control.
[a]From Bhat et al. (2001).
[b]From Hoshi et al. (2007).
[c]$P < 0.05$.

and Table IV), we show here a statistically significant 27% reduction in paranode length in a much larger sample of 3–7-month mice (*shaking*: 2.3 ± 0.8 μm, n = 76; control: 3.1 ± 0.7 μm, n = 65, $P < 0.05$).

DISCUSSION

In summary, this study has shown the following:

1. 10 kDa dextran penetration of control paranodes is similar to that by 3 kDa dextran. 40 kDa dextran penetration is similar to that by 70 kDa dextran.

2. Dextran tracers penetrate the paranodes of myelinated *cst*-null and *Caspr*-null sciatic nerve fibers, which are deficient in TBs, to the same extent as in control mice, but penetration of *shaking* paranodes, despite large numbers of TBs, is increased compared with controls. Thus, absence of paranodal TBs does not increase penetration of these tracers.

3. In both mutant and control sciatic nerve fibers, dextran penetration is inversely proportional to paranode length and inversely proportional to paranodal axon diameter, both of which are linked to the length of the helical pathway 3 between the terminal loops of the PNJ through the paranode (see Fig. 1). The increased permeability of the shaking fibers can be directly attributed to its thinner myelin, shortened paranodes and attendant shortening of pathway 3.

4. Our findings are consistent with diffusion of the dextran tracers we used through the paranode via pathway 3 in both control and mutant fibers.

Effect of Tracer Size on Penetration of Paranodes

Our previous work demonstrated that both 3 kDa (d = ~26Å) and 70 kDa (d = ~118–162Å) particles were able to penetrate the paranode, apparently via the helical pathway between paranodal loops rather than directly through the PNJ cleft, based on diffusion calculations (Mierzwa et al., 2010b). The 3 kDa tracer, how-

ever, penetrated the paranode to a greater extent and in a larger proportion of the fibers, whereas entry of the 70 kDa tracer was restricted to very few paranodes. Here we show comparable results with tracers of intermediate size −10 kDa ($d = {\sim}46\text{Å}$) and 40 kDa ($d = {\sim}90\text{–}146\text{Å}$). We did not find an absolute "cut-off" size for tracer penetration, but we did find a marked reduction in distance moved and number of paranodes penetrated going from the 10 kDa tracer to the 40 kDa tracer, consistent with a partial "filter" somewhere between those two sizes.

Although penetration of other molecules would depend on additional parameters, including shape and charge, we can at least say, based on penetration by the relatively inert dextran molecules, that particles and cell processes larger than ${\sim}100\text{–}150\text{Å}$ in diameter would be largely excluded by the PNJ. This might include IgMs, complement components, virions and cellular pseudopodia. Conversely, widening of the junctional cleft or of the diameter of pathway 3 and shortening of pathway 3 would be expected to increase access of those elements to the internodal region of the axon.

Pathways for Penetration

In our previous study (Mierzwa et al. 2010b), we suggested three possible routes of diffusion through the paranode. Our data supported diffusion of dextran tracers through pathway 3 between the paranodal loops. The current results bolster our earlier hypothesis in two ways:

1. Dextran penetration varies with axon diameter, which, in turn, affects the length of pathway 3. In a fiber with a paranode 3 μm long, an increase in axon diameter from 5 μm to 6 μm would not significantly change the lengths of pathways 1 or 2 but would increase pathway 3 by ${\sim}94$ μm.[1] Thus, the only pathway significantly affected by increased axon diameter is pathway 3.
2. Dextran diffusion is independent of the presence or absence of TBs. Our results, showing no difference in penetration in the *cst*-null mice (rare TBs) and *Caspr*-null mice (no TBs) underline the fact that the absence of these structures, which could affect pathways 1 and 2, but not pathway 3, does not change dextran penetration.

As noted above, the tight junction between adjacent loops at the apex of pathway 3 is not always present, especially where clusters of loops fail to reach the axolemma. In those cases, tracer would be expected to extend away from the axon into the interloop space up to the point where the loops form compact myelin lamellae. Pooling of tracer in the spaces around the loops that

fail to reach the axolemma probably underlies the paranodal barb-like image sometimes seen in our fluorescent dextran studies, corresponding to a classical histological finding, the paranodal "spiny bracelet" (Nageotte, 1922).

Comparable observations have also been made in studies of peroxidase penetration (Towfighi and Gonatas, 1977). In Fig. 5 of that article, horseradish peroxidase (HRP) reaction product can be seen between paranodal loops extending 7–8 loops in the abnodal direction, corresponding to pathway 3 (see Fig. 1) as well as in interloop spaces further removed from the axon. These results are consistent with our dextran data, but there is no indication of the proportion of fibers that showed penetration by HRP. That study also claimed penetration of the tracer, which approximates 50–60Å in diameter, into the paranodal junctional cleft, but that interpretation is complicated by three potential problems inherent in the peroxidase method:

1. The enzyme is not inert and in living tissue may open pathways that are normally closed.
2. Reaction product may diffuse from the locus of the peroxidase molecule (Courtoy et al. 1983; Dourmashkin et al. 1982; Novikoff et al. 1972), resulting in spurious localization.
3. Movement of the peroxidase molecule itself could occur *after* fixation during the prolonged preparation period required for electron microscopy processing (postfixation, rinsing, dehydration, and infiltration) before the tracer is fully stabilized by embedment in plastic.

The dextran tracers used in this and in our previous study (Mierzwa et al., 2010b) avoid these complications.

Penetration is Increased in the *Shaking Mutant*

The most striking finding of this study is the increased dextran penetration in the *shaking* mutant, in which TBs are abundant but which is less impaired neurologically and which has a longer life-span than the other mutants tested. The number of paranodal loops contacting the axon is a significant factor in determining the length of pathway 3 through the paranode, and the increased *g*-ratio in *shaking* fibers means fewer layers of myelin and thus fewer PN loops. For this reason, pathway 3 through the *shaking* paranode is shorter; hence the time taken to traverse it is correspondingly reduced and the distance moved at any given time increased.

Relation of Paranodal Structure to Permeability

Structural studies of mouse mutants lacking TBs have shown marked disorganization of paranodal structure in the CNS but only modest defects in the PNS. In the case of *cgt*-null mice, which lack TBs entirely, CNS paranode structure deteriorates gradually over time, resulting ultimately in gross abnormalities in nodal conformation

---

[1]Because pathway 3 moves virtually circumferentially around the axon, increasing axon *diameter* by 1 μm would result in lengthening pathway 3 between each pair of PN loops by the increase in axonal *circumference*, i.e. ${\sim}1$ μm $\times$ π. If each paranodal loop in contact with the axon is 0.1 μm in axial length, a 3-mm paranode would have 30 PN loops. The overall increase in pathway 3 length along the entire paranode would thus approximate 30×1 μm $\times$ π, or ${\sim}94$ μm.

and dimensions and a corresponding gradual increase in neurological deficits (Rosenbluth, 2009). Comparable changes occur in *cst*-null mice, which have small numbers of TBs, but in that mutant, deterioration progresses more slowly over a much longer time period (Marcus et al., 2006).

In both cases, surprisingly, many paranodal loops remain closely apposed to the axon in the short term (Bhat et al., 2001), although in *contactin*-null mice, which also lack TBs, the gap width appears to be increased (Boyle et al., 2001). To what extent the appearance of this apposition is dependent on specimen preparation is unknown.

Our expectation in the current study was that in the absence of TBs the PNJ gap might widen and become more permeable, resulting in increased penetration of the tracers we have used, in particular the 3 kDa dextran whose diameter approximates the width of the normal PNJ gap. Our results, however, show no evidence of dextran penetration beyond what is seen in control specimens. The implication of this finding is that the PNJ gap is occluded or that other mechanisms maintain the separation of the junctional membranes at a distance insufficient to accommodate these dextrans.

Functional Implications

Our data show that the ability of the dextrans to penetrate the paranode depends on its dimensions. Thus, any pathological process that results in shortening of paranodes, e.g., demyelination followed by thin remyelination, as seen in MS, or proteolysis of TBs, which might occur in the presence of inflammation and lead to retraction of adnodal PN loops, should decrease the length of pathway 3 and reduce the time for penetration of macromolecules to the juxtaparanode and internode. In MS shadow plaques, thinly remyelinated fibers with fewer paranodal loops and shortened paranodes might therefore be more susceptible to cytokines, granzyme and other molecules released by inflammatory cells that could penetrate more readily to the juxtaparanode and internode. Similarly, short paranodes could facilitate penetration of immunoglobulins to juxtaparanodal or internodal targets, as occurs in acute motor neuropathy (Hafer-Macko et al., 1996) and neuromyotonia (Kleopa et al., 2006).

Shortening of this pathway would also increase its electrical conductance resulting in increased passive current flow between the node and the juxtaparanodal K+ channels, thus increasing their influence on nodal excitability. This could have the effect of dampening nodal excitability, diminishing nodal action currents, compromising the ability of nodes to follow at high frequency, diminishing passive currents to adjacent nodes, lengthening of their time to reach threshold and thus slowing conduction (Rosenbluth, 2009), all of which could have significant functional consequences.

REFERENCES

Berthold CH, Rydmark M. 1983. Anatomy of the paranode–node–paranode region in the cat. Experientia 39:964–976.

Bertram M, Schroder JM. 1993. Developmental changes at the node and paranode in human sural nerves: Morphometric and fine structural evaluation. Cell Tiss Res 273:499–509.

Bhat MA, Rios JC, Lu Y, Garcia-Fresco GP, Ching W, St Martin M, Li J, Einheber S, Chesler M, Rosenbluth J, Salzer JL, Bellen HJ. 2001. Axon–glia interactions and the domain organization of myelinated axons requires neurexin IV/Caspr/Paranodin. Neuron 30:369–383.

Boyle ME, Berglund EO, Murai KK, Weber L, Peles E, Ranscht B. 2001. Contactin orchestrates assembly of the septate-like junctions at the paranode in myelinated peripheral nerve. Neuron 30:385–397.

Courtoy PJ, Picton DH, Farquhar MG. 1983. Resolution and limitations of the immunoperoxidase procedure in the localization of extracellular matrix antigens. J Histochem Cytochem 31:945–951.

Devaux J, Gow A. 2008. Tight junctions potentiate the insulative properties of small CNS myelinated axons. J Cell Biol 183:909–921.

Dourmashkin R, Patterson S, Shah D, Oxford JS. 1982. Evidence of diffusion artefacts in diaminobenzidine immunocytochemistry revealed during immune electron microscope studies of the early interactions between influenza virus and cells. J Virol Methods 5:27–34.

Einheber S, Zanazzi G, Ching W, Scherer S, Milner TA, Peles E, Salzer JL. 1997. The axonal membrane protein Caspr, a homologue of neurexin IV, is a component of the septate-like paranodal junctions that assemble during myelination. J Cell Biol 139:1495–1506.

Feder N. 1971. Microperoxidase: An ultrastructural tracer of low molecular weight. J Cell Biol. 51:339–343.

Gollan L, Salomon D, Salzer JL, Peles E. 2003. Caspr regulates the processing of contactin and inhibits its binding to neurofascin. J Cell Biol 163:1213–1218.

Hafer-Macko C, Hsieh ST, Li CY, Ho TW, Sheikh K, Cornblath DR, McKhann GM, Asbury AK, Griffin JW. 1996. Acute motor axonal neuropathy: an antibody-mediated attack on axolemma. Ann Neurol 40:635–644.

Hall SM, Williams PL. 1971. The distribution of electron dense tracers in peripheral nerve fibers. J Cell Sci 8:541–555.

Hirano AN, Becker H, Zimmerman HM. 1969. Isolation of the pereiaxonal space of the central myelinated nerve fiber with regard to the diffusion of peroxidase. J Histochem Cytochem 17:512–516.

Honke K, Hirahara Y, Dupree J, Suzuki K, Popko B, Fukushima K, Fukushima J, Nagasawa T, Yoshida N, Wada Y, Taniguchi N. 2002. Paranodal junction formation and spermatogenesis require sulfoglycolipids. Proc Natl Acad Sci U S A 99:4227–4232.

Hoshi T, Suzuki A, Hayashi S, Tohyama K, Hayashi A, Yamaguchi Y, Takeuchi K, Baba H. 2007. Nodal protrusions, increased Schmidt–Lanterman incisures, and paranodal disorganization are characteristic features of sulfatide-deficient peripheral nerves. Glia 55:584–594.

Hrabetova S. 2005. Extracellular diffusion is fast and isotropic in the stratum radiatum of hippocampal CA1 region in rat brain slices. Hippocampus 15:441–450.

Ishibashi T, Dupree JL, Ikenaka K, Hirahara Y, Honke K, Peles E, Popko B, Suzuki K, Nishino H, Baba H. 2002. A myelin galactolipid, sulfatide, is essential for maintenance of ion channels on myelinated axon but not essential for initial cluster formation. J Neurosci 22:6507–6514.

Kleopa KA, Elman LB, Lang B, Vincent A, Scherer SS. 2006. Neuromyotonia and limbic encephalitis sera target mature Shaker-type K+ channels: Subunit specificity correlates with clinical manifestations. Brain 129:1570–1584.

MacKenzie ML, Ghabriel MN, Allt G. 1984. Nodes of Ranvier and Schmidt–Lanterman incisures: An in vivo lanthanum tracer study. J Neurocytol 13:1043–1055. www.springerlink.com/index/K03X50VH 3L151468.pdf

Marcus J, Honigbaum S, Shroff S, Honke K, Rosenbluth J, Dupree JL. 2006. Sulfatide is essential for the maintenance of CNS myelin and axon structure. Glia 53:372–381.

Mierzwa A, Arevalo JC, Chao M, Rosenbluth J. 2005. Evidence for myelin instability in a shaking mouse mutant. Soc. Neuroscience, annual meeting, Washington, DC Poster 277.17.

Mierzwa A, Arevalo JC, Schiff R, Chao M, Rosenbluth J. 2010a. Role of transverse bands in maintaining paranodal structure and axolemmal domain organization in myelinated nerve fibers: effect on longevity in dysmyelinated mutant mice. J Comp Neurol 518:2841–2853.

Mierzwa A, Shroff S, Rosenbluth J. 2010b. Permeability of the paranodal junction of myelinated nerve fibers. J Neurosci 30:15962–15968.

Nageotte J. 1922. L'organisation de la matière dans ses rapports avec la vie. Paris: Librairie F. Alcan.

Nicholson C, Tao L. 1993. Hindered diffusion of high molecular weight compounds in brain extracellular microenvironment measured with integrative optical imaging. Biophys J 65:125–134.

Novikoff AB, Novikoff PM, Quintana N, Davis C. 1972. Diffusion artifacts in 3, 3′ diaminobenzidine cytochemistry. J Histochem Cytochem 20:745–749.

Pannese E. 1994. Neurocytology. Fine structure of neurons, nerve processes and neuroglial cells, Stuttgart: Georg Thieme Verlag.

Poliak S, Peles E. 2003. The local differentiation of myelinated axons at the nodes of Ranvier. Nat Rev Neurosci 4:968–980.

Reier P, Tabira T, Webster H deF. 1976. The penetration of fluorescein-conjugated and electron dense tracer proteins into Xenopus tadpole optic nerves following perineural injection. Brain Res 102:229–244.

Rosenbluth J. 1976. Intramembranous particle distribution at the node of Ranvier and adjacent axolemma in myelinated axons of the frog brain. J Neurocytol 5:731–745. www.springerlink.com/index/K7118706066T4646.pdf.

Rosenbluth J. 2009. Multiple functions of the paranodal junction of myelinated nerve fibers. J Neurosci Res 87:3250–3258.

Salzer JL, Brophy PJ, Peles E. 2008. Molecular domains of myelinated axons in the peripheral nervous system. Glia 56:1532–1540.

Shepherd MN, Pomicter AD, Velazco CS, Henderson SC, Dupree JL. 2010. Paranodal reorganization results in the depletion of transverse bands in the aged central nervous system. Neurobiol Aging [Epub ahead of print].

Syková E, Nicholson C. 2008. Diffusion in brain extracellular space. Physiol Rev 88:1277–1340.

Thorne R, Nicholson C. 2006. In vivo diffusion analysis with quantum dots and dextrans predicts the width of brain extracellular space. Proc Nat Acad Sci USA 103:5567–557.

Towfighi J, Gonatas N. 1977. The distribution of peroxidases in sciatic nerves of normal and hexachlorophene-intoxicated developing rats. J Neurocytol 6:39–47.www.springerlink.com/index/j550v11k923047t7.pdf.